View metadata, citation and similar papers at core.ac.uk

brought to you by CORE

provided by Electronic Publication Information Center

AGU PUBLICATIONS

Geochemistry, Geophysics, Geosystems

TECHNICAL REPORTS: DATA

10.1002/2016GC006750

Key Points:
- Robust plate tectonic models provide the necessary information to produce maps of seafloor age
- We present a new high-resolution seafloor age grid for the South Atlantic based on the kinematic model of *Pérez-Díaz and Eagles* [2014]
- Identifying and quantifying the uncertainties involved in our workflow allows us to estimate age grid accuracy

Supporting Information:
- Supporting Information S1
- Figure S1
- Data Set S1
- Data Set S2
- Data Set S3
- Data Set S4

Correspondence to:
L. Pérez-Díaz,
lucia.perezdiaz@rhul.ac.uk

Citation:
Pérez-Díaz, L., and G. Eagles (2017), A new high-resolution seafloor age grid for the South Atlantic, *Geochem. Geophys. Geosyst.*, *18*, doi:10.1002/2016GC006750.

Received 29 NOV 2016
Accepted 5 JAN 2017
Accepted article online 10 JAN 2017

© 2017. American Geophysical Union. All Rights Reserved.

A new high-resolution seafloor age grid for the South Atlantic

L. Pérez-Díaz[1] and G. Eagles[2]

[1]Royal Holloway University of London, Surrey, UK, [2]Alfred Wegener Institute, Helmholtz Centre for Polar and Marine Research, Bremerhaven, Germany

Abstract Digital grids of basement age of the world's oceans are essential for modern geodynamic and paleoceanographic studies. Any such grid is built using a plate kinematic model, whose accuracy and reliability directly influence the accuracy and reliability of the grid. We present a seafloor age grid for the South Atlantic based on a recent high-resolution plate kinematic model. The grid is built from a data set of points whose ages are defined in or for the plate kinematic model, incorporating breaks at tectonic boundaries like fracture zones where the age function is discontinuous. We compare predictions of the new grid and of a previously published one, which is based on an older plate kinematic model, to magnetic isochron pick data sets. The comparison shows the new grid to provide a more reliable depiction of seafloor age in the South Atlantic. Numerical estimates of the new grid's uncertainty are determined by interpolation between (1) misfits at grid cells coinciding with magnetic isochron ages, (2) misfits implied by locational uncertainties in predicted isochrons propagated from uncertainties in the plate kinematic model, and (3) by the proximities of cells to fracture zone traces or ridge-jump scars. Estimated total uncertainty is <10 My for 94% of the grid and <5 My for 72%, but much larger in areas where magnetic anomaly data are scarce (such as the Cretaceous Normal Superchron) and in the vicinity of long-offset fracture zones.

1. Introduction

In recent times, tectonic models describing the opening of the South Atlantic have proliferated [e.g., *Schettino and Scotese*, 2005; *König and Jokat*, 2006; *Eagles*, 2007; *Torsvik et al.*, 2009; *Moulin et al.*, 2010; *Heine et al.*, 2013]. Each of these models provides a context within which to interpolate between locations of known seafloor age and so, potentially, to produce a grid of the age of oceanic lithosphere.

Age grids are applied in a range of plate kinematic and geodynamic studies. Notably, they are used to portray variations in the direction and rate of seafloor spreading over large areas [e.g., *Müller et al.*, 2008]. They are also used to determine the depth to the top surface of a thermally subsiding lithosphere, of which the differences to measured bathymetry are important in studies of dynamic topography, crustal thickness variation, sediment thickness, and paleobathymetry (e.g., Pérez Díaz and Eagles, Modelling paleobathymetry: a method based on South Atlantic data, submitted to *Geol. Soc. of London Special Publication*, 2017).

Given their basis, the reliabilities of age grids depend on the choice of underlying plate kinematic model. A series of global seafloor age grids have been produced since the 1990s and published as stand-alone products [*Müller and Roest*, 1997; *Müller et al.*, 2008] or as data supplements to papers dealing with global plate kinematics [e.g., *Müller et al.*, 2016]. In the South Atlantic, these grids are based on the plate kinematic study of *Nürnberg and Müller* [1991] and, more recently, modifications made to it by *Heine et al.* [2013] to make it compatible with their determinations of intracontinental rifting processes and the location of the continent-ocean boundary.

In the following, we detail the steps involved in generating an alternative high-resolution gridded age map for the South Atlantic derived from the more up-to-date and precise kinematic model of *Pérez-Díaz and Eagles* [2014], critically examining its uncertainties and limitations.

2. Method

Our grid (Figure 1b) is based on a large data set (Figure 1a) composed of (1) 15,407 points interpolated onto isochrons constrained within the model of *Pérez-Díaz and Eagles* [2014] and 87,660 points interpolated at 1 My intervals between them, (2) a set of fracture zone traces (gray lines in Figure 1a) digitized from satellite

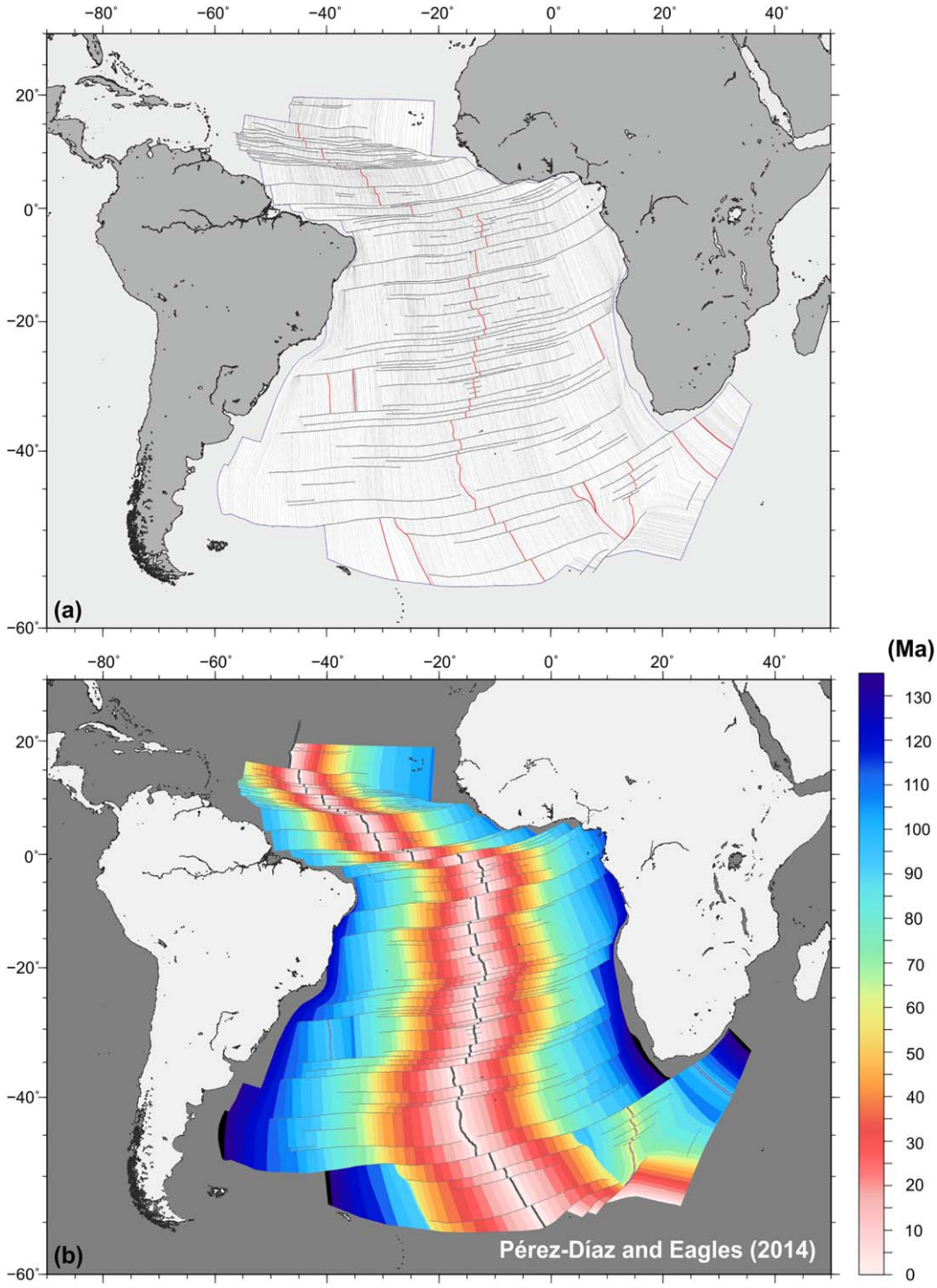

Figure 1. (a) Age points (black), fracture zone traces (gray lines), and various tectonic boundaries (red lines) used to generate the age grid. (b) Seafloor age grid of the South Atlantic derived from the kinematic model of *Pérez-Díaz and Eagles* [2014]. Present-day mid-ocean ridge is shown as paired parallel black lines; fossil spreading centers shown as paired parallel blue lines.

altimeter data [*Sandwell and Smith*, 2014], and (3) a set of other tectonic boundaries (mid-ocean ridges, extinct ridge crests, and triple junction traces; red lines in Figure 1a).

Isochron ages were assigned according to the magnetic reversal time scale of *Gradstein et al*. [2004]. Interpolation was done visually between these isochrons, guided by seafloor gravity fabric and the need for isochrons to unite at paleo-ridge crests.

Fracture zones were picked and interpolated by hand. The locations of the resulting fracture zone traces typically differ by less than 10 km from locations picked automatically following the procedure of *Wessel* et al. [2015]. This value is comparable to the absolute reliability in the location of a fracture zone axis picked from satellite gravity data [*Müller et al*., 1991], and considerably less than the total width of a typical fracture zone-related gravity anomaly. The choice of fracture zone mapping technique is therefore unlikely to be of significance for confident interpretation of the grid.

Seafloor age is interpolated according to minimum curvature rules using a contouring and surface modeling software package (Surfer 13, Golden Software). Minimum curvature methods generate smooth surfaces that pass through or close to a set of input data points in such a way that the amount of bending on the surface is reduced to a minimum. No interpolation is calculated for portions of the grid that cross the digitized fracture zone traces, so that they act as explicit breaks in the age function. We set our interpolation to complete after 10,000 iterations, by which time the change in overall misfit of the surface to the input data points between iterations is insignificantly ($\ll$0.02 My) small with respect to the accuracy of dated reversals in the *Gradstein et al*. [2004] magnetic time scale, and to populate the grid at 1 arc min spacing. In many areas, the low density of age data points means the results of the minimum curvature algorithm approximate a linear interpolation.

2.1. Comparison With Other Age Grids

With the improvement in magnetic anomaly data quality and increase in quantity, the availability of more sophisticated kinematic models, and increases in computing power and software capabilities, printed maps of magnetic anomaly isochrons [e.g., *Sclater et al*., 1981; *Larson et al*., 1985] gave way to continuous digital age grids of the world's oceans [e.g., *Müller and Roest*, 1997]. *Müller et al*. [2008] presented an updated version of this data set, which *Müller et al*. [2016] further refined. In the South Atlantic, the refinements to these models have mostly intended to take account of new interpretations of the location and age of the continent-ocean boundary [e.g., *Heine et al*., 2013], so that it smoothly transitions to the oceanic crustal ages defined by the plate kinematic model of *Nürnberg and Müller* [1991]. In contrast, our age grid is based on the more recent kinematic model of *Pérez-Díaz and Eagles* [2014]. That model is not led by interpretations of the age or location of the continent-ocean boundary, which are subject to uncertainties in the region of 5 My and 200 km [*Eagles et al*., 2015].

The differences between the new seafloor age grid and those of *Müller et al*. [2016] are shown in Figure 2b. Small differences along the margins illustrate the uncertainties in these areas resulting from the limited numbers of magnetic isochron data. The well-known south-north propagation of the mid-ocean ridge during ocean opening is depicted most starkly by the age grid of *Pérez-Díaz and Eagles* [2014]. Further large differences feature for the regions of the Vema Channel and Southern Ocean Large Igneous Province ridge jumps interpreted by *Pérez-Díaz and Eagles* [2014] (Figure 2b). Similarly, the location of the fossil boundaries of the Malvinas plate, especially that with the South American plate, results in large predicted age differences.

These differences show that the choice of age grid is a source of uncertainty. This uncertainty might affect studies that use age grids for calculating plate divergence rates [e.g., *Brune* et al., 2016], or for making paleobathymetric maps [e.g., *Baatsen* et al., 2016]. In the latter, for example, the age differences of 18 My in the equatorial Atlantic imply that paleobathymetry calculated there for mid-Cretaceous times might be in error by as much as 1.6 km.

To compare the relative fidelities of the new grid and that of *Müller et al*. [2016], Figure 3b shows misfits between the ages assigned to picks in the magnetic anomaly data set used by *Pérez-Díaz and Eagles* [2014] (shown in Figure 3a) to the ages predicted by the two age grids for the locations of those magnetic anomaly picks. Overall, misfits defined with *Müller* et al. [2016] are slightly more broadly distributed (standard deviation of 3.0 My compared to 2.6 My), and the distribution shows positive skewness as opposed to the more symmetrical distribution of misfits to the new grid. The differences lie within the range of resolvable ages based on uncertainties in the *Gradstein et al*. [2004] time scale, on which our grid's ages are based, and so can be regarded as significant.

Figure 4 shows a more objective fidelity test, using a data set of age points consisting of one radiometric age determination from DSDP Site 355 in the Brazil Basin, and 130 new magnetic isochron picks made in

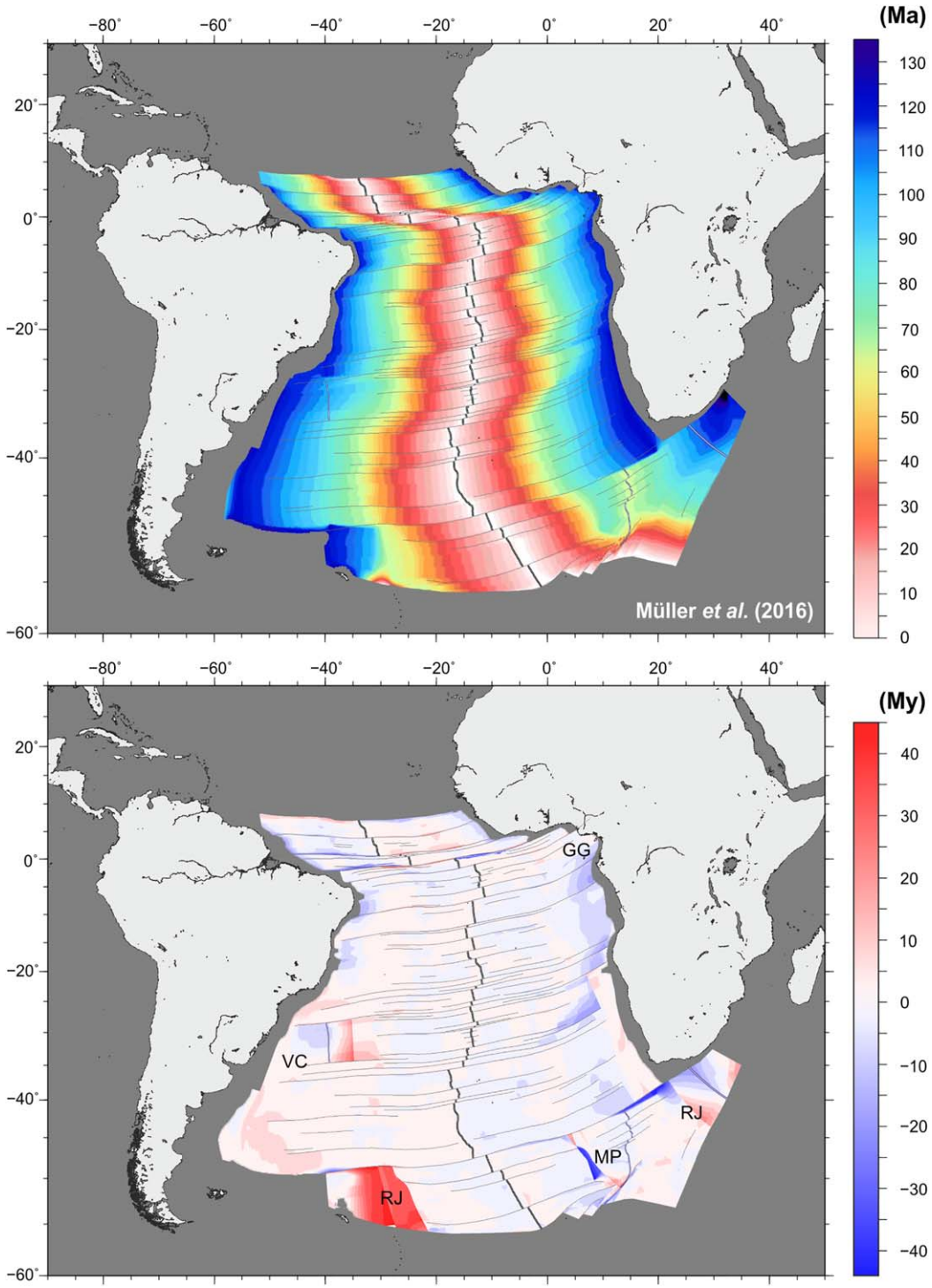

Figure 2. (a) Seafloor age grid of *Müller et al*. [2016]. Mid-ocean ridge, fossil spreading centers and fracture zone traces as interpreted by *Pérez-Díaz and Eagles* [2014]. Color key as in Figure 1. (b) Differences between the seafloor age grid of *Müller et al*. [2016] and our new grid. Warm colors denote areas where the new grid predicts older seafloor than that of *Müller et al*. [2016] and vice versa. GG: Gulf of Guinea; MP: Malvinas Plate; RJ: Southern Ocean Large Igneous Province ridge jump; VC: Vema Channel Ridge Jump.

helicopter and shipborne data from the Argentine and Cape basins [*Jokat*, 2009, 2013]. None of these data were used in determining the rotations of *Nürnberg and Müller* [1991] or the rotations of *Pérez-Díaz and Eagles* [2014], and none of these data were used as input points for surface fitting to produce any of the age grids cited or discussed here. As such, the distribution of misfits between these points and any age grid

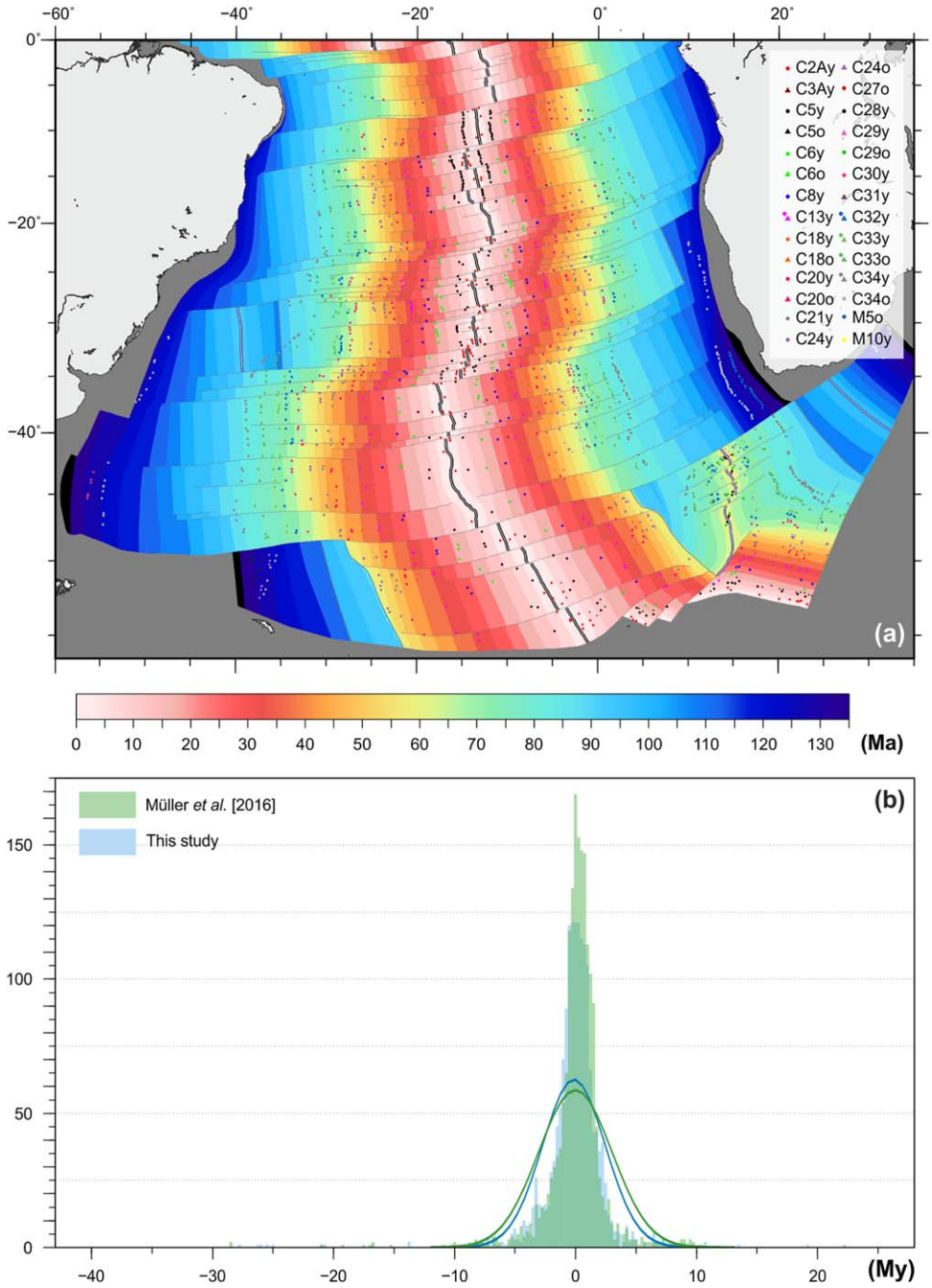

Figure 3. (a) Disks: Magnetic anomaly identifications used to constrain the kinematic model of *Pérez-Díaz and Eagles* [2014] (from *Cande* et al. [1988] *Shaw and Cande* [1990], *Nankivell* [1997], and *Eagles* [2007]). Triangles: other identifications from those studies and from *Marks and Stock* [2001] that did not contribute to the kinematic model. Color scale and background age grid as in Figure 1. (b) Histogram showing the distribution of calculated differences between ages assigned to the anomaly identifications and at the corresponding points in the new age grid and that of *Müller et al*. [2016]. Ages assigned according to the magnetic anomaly reversal time scales of *Gradstein et al*. [2004] for the new grid and *Gee and Kent* [2007] for *Müller et al.*'s [2016] age grid. Color bars are semitransparent to enable comparison of the histograms for the two age grids. Green and blue lines show the best-fitting Gaussian distributions to the misfit populations calculated with *Müller et al*. [2016] and in this study.

should be a reliable guide to that grid's usefulness as a predictive tool for seafloor age. Of the two, the distribution of misfits to our new grid more closely resembles a normal distribution, and is furthermore slightly (standard deviation 2.1 My versus 2.4 My) but nonetheless, with respect to time scale accuracy, significantly tighter than that of misfits to *Müller et al*. [2016].

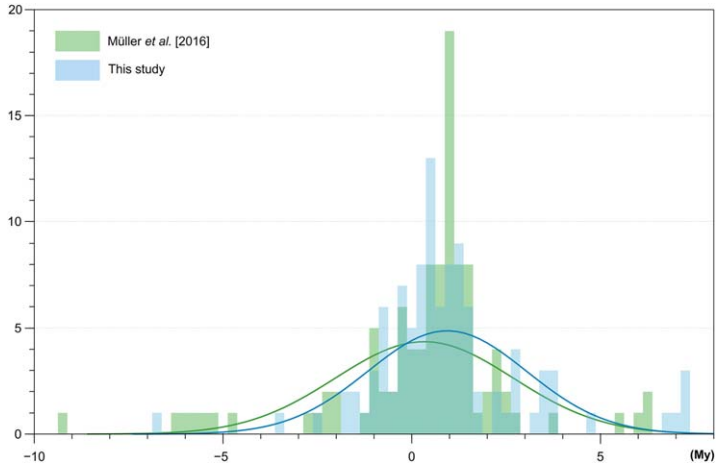

Figure 4. Histogram showing the distribution of calculated differences between ages assigned to 130 new magnetic isochron picks made in helicopter and shipborne data [*Jokat*, 2009, 2013] and by our age grid and that of *Müller et al*. [2016]. Color bars are semi-transparent to enable comparison of the histograms for the two age grids. Green and blue lines show the best-fitting Gaussian distributions to the misfit populations calculated with *Müller et al*. [2016] and in this study.

3. Sources of Age Uncertainty

The age of the ocean floor plays an essential role in studies of plate kinematics, plate driving forces, mantle dynamics, and paleoceanography. For this reason, it is important to understand the uncertainties and limitations involved in the process of modeling seafloor age. The minimum uncertainty in the age assigned to any point on a map of oceanic lithosphere can be determined by one or more of the following considerations.

1. At points constrained by magnetic wiggle isochrons, the greater of (a) the uncertainty in location of the point on the wiggle trace that is given an isochron age (navigational and process-related uncertainty in location); or (b) the uncertainty in age assigned to the isochron from a chosen time scale.

   Locational inaccuracies in the collection of magnetic data are related to the accuracy of navigation techniques at the time the data were collected, and to the skewness of magnetic anomalies recorded in an inclined geomagnetic field. Most of the magnetic isochron identifications in Figure 3a were acquired between 1958 and 1981 [*Cande et al*., 1988; *Shaw and Cande*, 1990], using pre-GPS navigational techniques for which conservative positional error estimates lie in the region of 5–15 km [*Kirkwood et al*., 1999]. This uncertainty is greater than or similar in magnitude to what might be expected from uncorrected skewness in magnetic profiles. These uncertainties in turn are potentially smaller than those one might expect from geological processes related to crustal accretion [e.g., *Parmentier and Forsyth*, 1985; *Smith et al*., 1999]. Given their size, locational uncertainties are likely to dominate in areas of high gradient in the age grid, or where the underlying kinematic model is based on interpretations of magnetic anomaly isochrons from particularly old magnetic data.

   The magnetic anomaly reversal time scale used here is that of *Gradstein et al*. [2004]. The process of magnetic reversal is thought to complete over the course of a few thousand years and can be considered geologically as instantaneous. Ages are assigned to these instants on the basis of radiometric ages determined from volcanic rocks in continuous sequences displaying reversals, and are usually quoted with numerical uncertainties. These errors are typically less than 0.5 My for the oldest (Mid-Cretaceous) isochrons of the South Atlantic, and decrease for younger ages. Because of this, it is unlikely that time scale-related uncertainties dominate anywhere in the grid.
2. At points constrained by plate-kinematically modeled isochrons (e.g., the kinematic model's C13 rotation predicts loci with an age of 33.5 Ma), some value determined by the uncertainty in the kinematic model.

   The kinematic model of *Pérez-Díaz and Eagles* [2014] was designed to closely replicate the locations of available seafloor spreading data, achieving a misfit population with a standard deviation of 22.5 km. Based on this value alone, the locations of age points predicted at the times of constrained rotations in the kinematic model can be expected to be slightly less reliable than those of the picked locations. In more detail, the model rotation poles also feature a set of 95% confidence regions that can be used to estimate the locational uncertainty of any predicted isochron pick. As before, the associated uncertainty in age is related to the gradient of the age grid.
3. At points constrained by interpolation by eye (i.e., by drawing the masks for times between the model-constrained isochrons), some value related to the distance over which interpolation is made.
4. At points constrained by interpolation by the minimum curvature algorithm between masks, some value related to the distance over which interpolation is made.

5. At points near fracture zones and other age discontinuities, some value related to the magnitude of the age offset across the discontinuity, and to the uncertainty in its location.

As a first estimate of the effects of all these considerations in terms of age, the misfit distributions in Figure 3b are made up of 88% of points that fall within a ~3 My error, and 96% within 6 My.

Figures 5 and 6 illustrate the distribution of the larger (>3 My) misfits to our age grid in order to help assess their likely causes. Likely examples of both navigational and geological process-related errors can be seen in Figure 5a. The first are of smaller magnitude and can be identified easily in areas where a series of magnetic anomaly identifications appear aligned, contrary to expectations, across a fracture zone (see, e.g., 26°W, 30°S). The cluster of large misfits centered at 35°W, 33°S is the result of *Pérez-Díaz and Eagles* [2014] interpretation, after presenting their inversion of the isochron pick data, of this area having been affected by a ridge jump. Under this interpretation, these anomalies characterize seafloor that was transferred from the African plate to the South American plate east of the Vema channel at 93 Ma, and were erroneously identified for the inversion as isochrons C33 and C34y. Consistent with this, the picks of anomaly C33y align along a basement ridge, whose gravity signature can be seen in Figure 5b.

The largest age discrepancies in Figure 6 are also located in the vicinity of another mid-ocean ridge jump along the Falkland Agulhas Fracture Zone in an area where volcanism postdated spreading [*Crough et al.*, 1980; *Hartnady and le Roex*, 1985; *Small*, 1995; *Le Roex et al.*, 2010]. Although it is possible that the Malvinas-South America plate boundary has been wrongly identified here (we did this following *Marks and Stock* [2001]), erroneous magnetic anomaly identifications are a plausible explanation for the age differences between magnetic chrons and the age grid in this region.

3.1. Error Estimates

To generate a grid of age uncertainty, we use the following procedure based on the considerations given above. In essence, it resembles that described by *Müller et al.* [2008] and used for the most recent version of

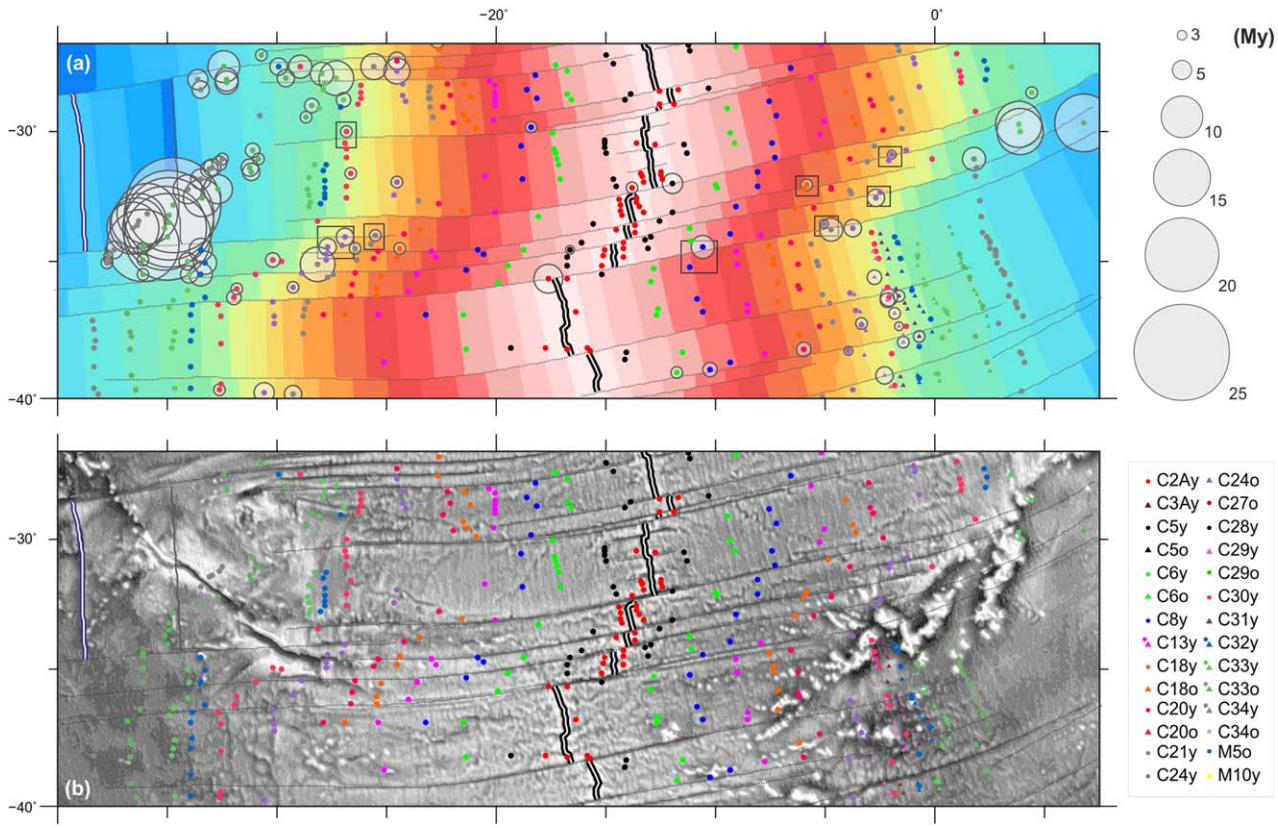

Figure 5. (a) Magnetic data and gridded age errors are plotted here over a gridded age map and (b) free-air gravity anomaly data. Squares: examples of errors arising from magnetic picks assigned in profiles situated on the opposite side of a fracture zone than neighboring picks of the same age. Color key as in Figure 1, symbol key as in Figure 5.

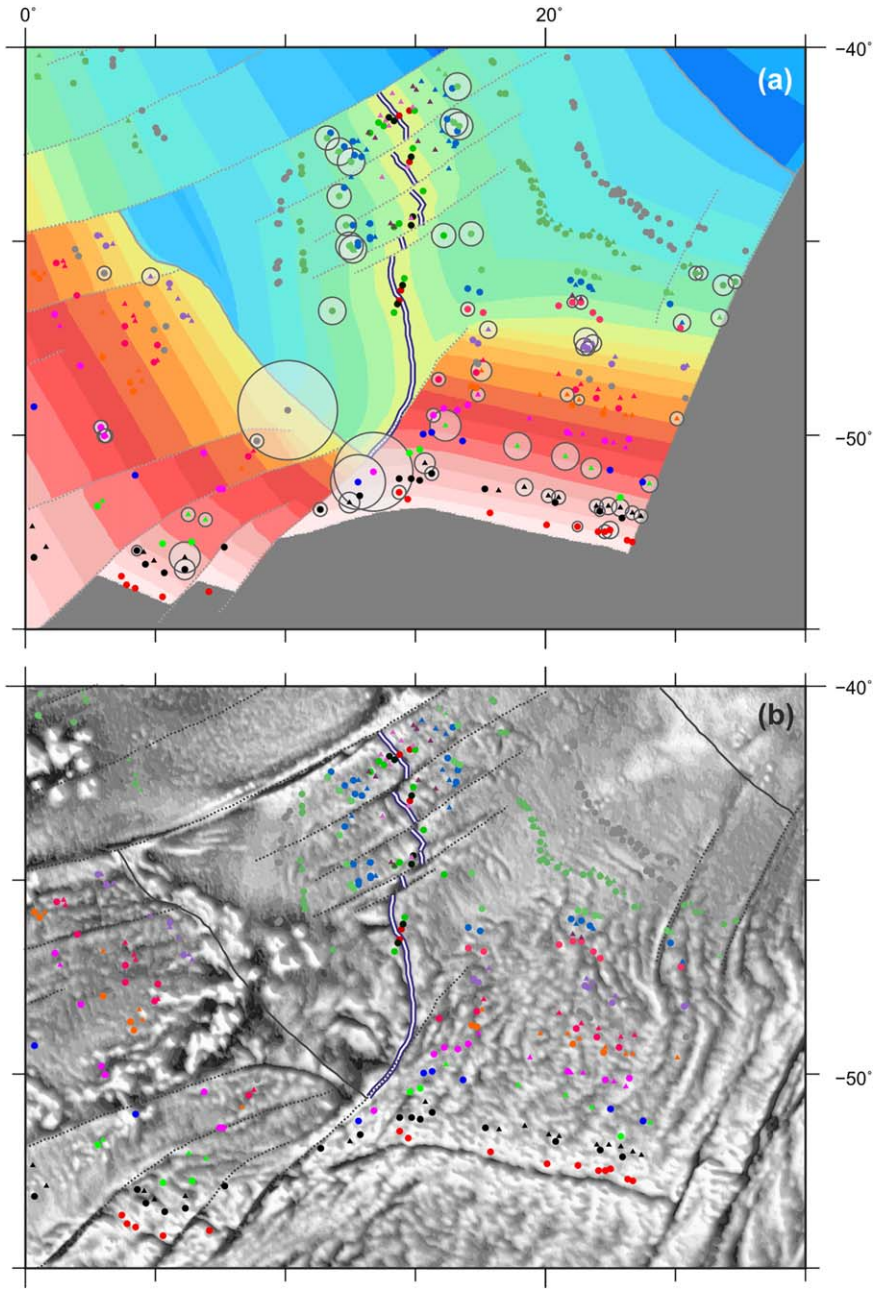

Figure 6. (a) Magnetic data and gridded age errors plotted over a gridded age map. (b) Magnetic data and gridded age errors plotted over free-air gravity anomaly data. Color key as in Figure 1; symbols as in Figure 5.

their grid, except for our use of the 95% confidence estimates in the kinematic model [*Pérez-Díaz and Eagles*, 2014]. *Müller et al.'s* [2008, 2016] grids assume their predicted isochron locations, from the visual fit model of *Nürnberg and Müller* [1991], to be equally reliable constraints as the magnetic isochron picks it was built from. Our consideration of the likely effect of uncertainties in the locations of the rotation poles propagating through to our age grid means that our uncertainty grid is likely to be more conservative and realistic than that of *Müller et al*. [2008].

3.1.1. Distance to Points of Constrained Age

Age grid uncertainty will be least for age grid cells containing magnetic isochron picks. In those cases, we estimate the uncertainty based solely on the differences between magnetic isochron ages and gridded age. The majority of these differences (located and summarized in Figures 3–6) fall within ±3 My, and only 3.3%

exceed ±6 My (two standard deviations). We suggested above that many of these might be explained in terms of errors in the magnetic isochron pick data set, rather than the age grid.

The kinematic model of *Pérez-Díaz and Eagles* [2014] has been shown to closely replicate the available seafloor spreading data, and can therefore be used to estimate (at least to some extent) the uncertainties in areas where magnetic data are scarce. To do this, we extract a data set of locations predicted to lie along magnetic isochrons constrained in the kinematic model of *Pérez-Díaz and Eagles* [2014]. Centered on each of these locations, we calculate a 95% elliptical confidence locus by propagation of the kinematic model's confidence estimates, within which the difference between the maximum and minimum ages in the age grid are taken as estimates of the age uncertainty. For the 2188 ellipses, whose semimajor axes vary between 5 and 20 km, the implied uncertainties are all smaller than 10 Ma. Only 29 points exceed 3 My uncertainty.

For age grid cells not coincident with magnetic or rotation-derived data points, the uncertainty will increase with interpolation distance from the nearest of such points. The greatest of these uncertainties exist for seafloor that formed during the Cretaceous Normal Superchron (CNS, 121-84 Ma) for which there are no magnetic isochrons and the nonmagnetic isochrons used to constrain early rotations by *Pérez-Díaz and Eagles* [2014] (ASM, NBU) are not dated with known precision.

These estimates are combined as follows. First, grid cells coincident with points of constrained age are given an error value equal to the misfit between our predicted ages and those assigned to magnetic anomaly identifications (Figures 5 and 6). The data set of points of constrained age used for this consists of (1) the sets of magnetic anomaly identifications used to calculate the rotation poles of *Pérez-Díaz and Eagles* [2014] and (2) a set of synthetic isochron points from the kinematic model of *Pérez-Díaz and Eagles* [2014]. Then, following *Müller et al.'s* [2008] treatment of interpolated age points, we allow uncertainty values to increase from the estimated errors at the constrained points to a maximum of 10 My greater than those errors at interpolated distances of 1000 km away from them.

3.1.2. Distance to Fracture Zone Traces

A further source of uncertainty in age estimates is to be expected in the areas of disturbed crust that comprise fracture zone traces, across which strong lateral contrasts in seafloor age occur. Magnetic or interpolated age estimates that are erroneously located on the "wrong" side of a fracture zone trace, whether as a result of navigational or digitization errors, will give rise to errors whose magnitude depends on the length of the transform fault at which the FZ formed.

Although the uncertainty in satellite fixes of fracture zone trough axes with respect to the deepest points in their topographic expressions is in the range of ±5 km [*Müller et al*., 1991], a more conservative estimate for the entire width of an average FZ anomaly in satellite gravimetry data is in the range of 20–30 km. With this in mind, we isolate areas around each FZ trace within which we apply a variable uncertainty value ranging from 0.5*x* My at a 25 km distance to *x* My at the FZ's axial trace. The value of *x* is the size of the age step (in My) from one side of a transform fault or FZ to the other, which depends on the length of the (paleo-)transform offset and paleo-spreading rates. The value of *x* varies between less than 1 My at short offset transforms and more than 40 My on parts of the Falkland-Agulhas FZ.

3.1.3. Total Age Grid Uncertainty

The grid shown in Figure 7a combines all of the uncertainty estimates described above. As such, this total uncertainty grid comprises constrained errors, given by discrepancies between the age grid and magnetic or kinematically modeled isochrons, proximity-based values interpolated between them, and values based on proximity to FZ traces. Figure 7b shows the distribution of these estimated total uncertainties. The distribution shows that total uncertainty is less than 10 My over 94% of the grid and less than 5 My for 72% of it. The map highlights how the largest uncertainties occur in areas formed during the CNS, and near tectonic age discontinuities such as the Falkland-Agulhas fracture zone and the Vema Channel ridge-jump scar.

4. Final Remarks

Seafloor age grids have a range of applications for studies of plate kinematics and plate driving forces. One example is in the calculation of seafloor spreading azimuths and rates from the two components of gradient vectors in an age grid. Figure 8 compares spreading directions calculated from our grid to those of *Müller et al.'s* [2016] grid. Gridding artifacts around the input data points appear as mottling in the difference grid.

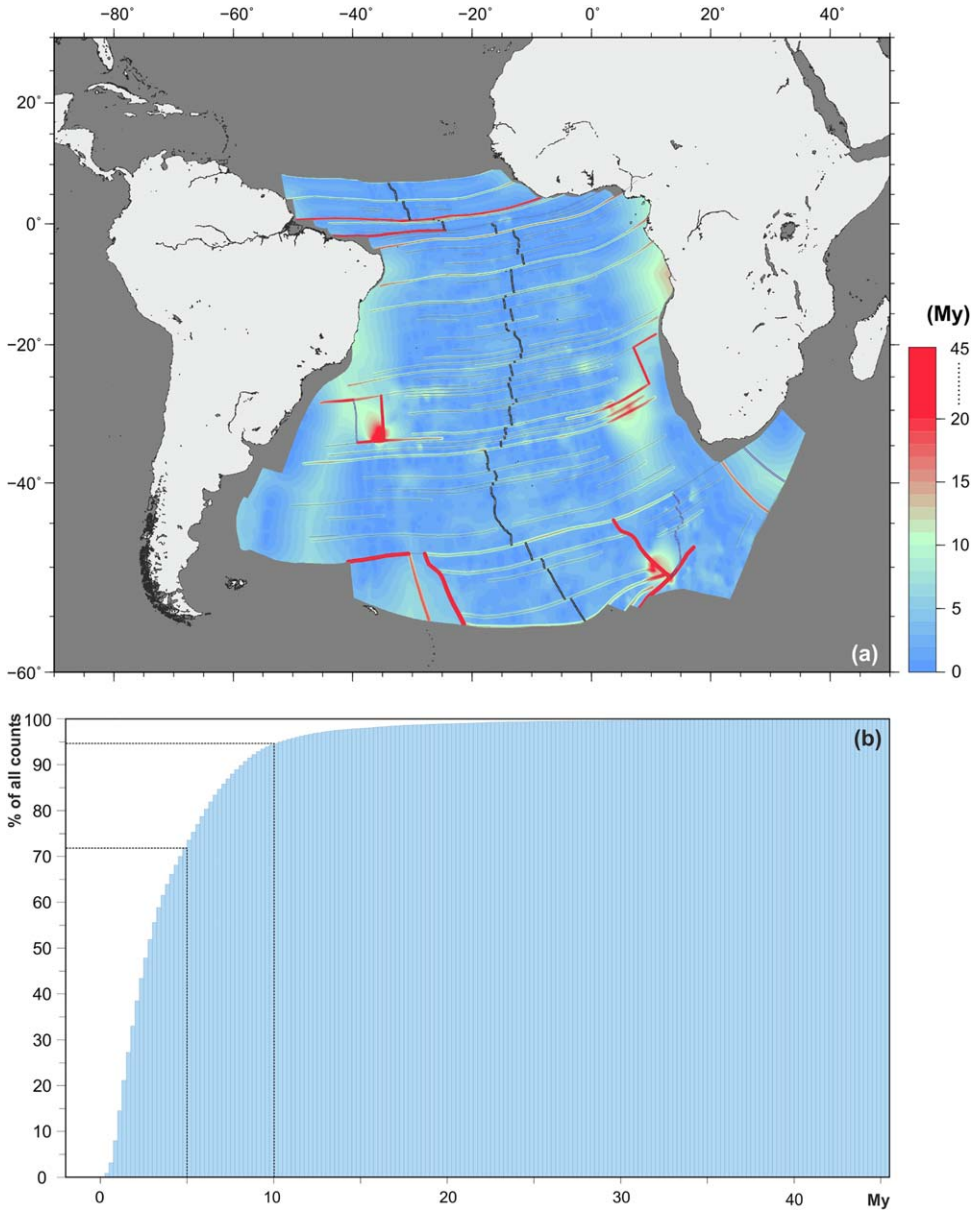

Figure 7. (a) Grid of total uncertainty in predicted ages calculated by considering, for each grid cell, the uncertainty resulting from its distance to points of constrained age and fracture zone traces. (b) Cumulative percentage of the distribution of uncertainties. Dotted lines highlight that 94% of the uncertainties' durations are 10 My or shorter, and that 72% are 5 My or shorter.

Larger areas of significant (>10°) divergence between the directions in the two grids are shown by gray colors in Figure 8c. The smallest of these occur across the two grids' contrasting sets of fracture zone location interpretations, of which the interpretations of *Müller* et al [2016] appear more prominent because of their global grid's coarser spatial resolution. In seafloor of the CNS, the two sets of fracture zone interpretations diverge by as much as 10°. At moderate wavelengths, the most striking differences are in the new grid's depiction of two areas of seafloor that have been exchanged between plates by long-range ridge jumps, identified by *Pérez-Díaz and Eagles* [2014] in the Vema Channel region and along the Falkland-Agulhas Fracture Zone. At long wavelengths, a ~10° difference in spreading direction between the kinematic models of *Nürnberg and Müller* [1991], which is not quantitatively constrained by fracture zone orientations, and *Pérez Díaz and Eagles* [2014], which is, is apparent through much of the South Atlantic's CNS-aged crust.

Figure 9 shows a comparison of spreading rates based on our new age grid and those of *Müller et al*. [2008, 2016]. The rates from the new grid and that of *Müller et al*. [2016] are calculated directly from the gradients

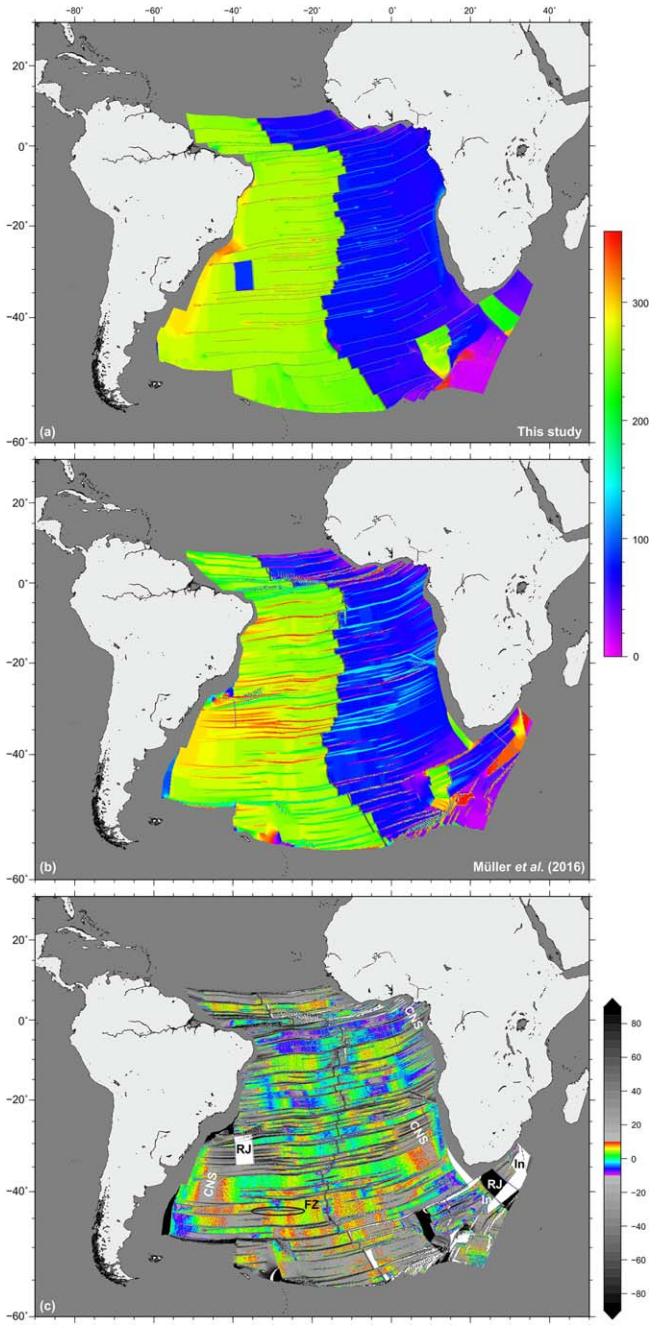

Figure 8. (a) Spreading directions derived from gradients in the age-grid of this study, (b) spreading directions of the age grid by *Müller et al.* [2016] and (c) grid of differences between (a) and (b). Labels to gray areas in Figure 8c: examples of large (<10°) differences arising from new interpretations of seafloor transfer between plates by ridge jumps (RJ), differences in spreading directions through the CNS modeled by *Nürnberg and Müller* [1991] and *Pérez-Díaz and Eagles* [2014] (CNS), long-distance interpolations in the *Müller et al.* [2016] grid (In), and variable interpretations of FZ locations (FZ).

of those age grids. NNW-directed smearing in the new grid reflects its construction by visual interpolation at 1 My intervals. Here it should be noted that any numerical comparison will be influenced by the fact that *Müller et al.*'s [2016] grid portrays ages, and therefore rates, according to the time scale of *Gee and Kent* [2007], *Müller et al.*'s [2008] according to the time scales of *Cande and Kent* [1995] and *Gradstein et al.* [1994], and ours according to *Gradstein et al.* [2004]. The various time scales are most similar for times since chron 34y (83 Ma), and accordingly the three studies portray similar post-Campanian histories, notably a long-lived period of slowing rates, starting at chron 33, that reach their nadir between chrons 30 and 24 [*Cande and Stegman*, 2011]. As with the seafloor spreading direction, larger differences are to be observed in the CNS-aged seafloor. Here the new grid shows rates that are considerably faster than in either *Müller et al.*'s [2008] or *Müller et al.*'s [2016] grid, an observation that can be considered robust alone if one considers the longer duration of the CNS in the *Gradstein et al.* [2004] time scale. These differences reflect the closer proximity of the South Atlantic to CNS-aged rotation poles in the kinematic models of *Nürnberg and Müller* [1991] and *Heine et al.* [2013] than to those of *Pérez-Díaz and Eagles* [2014]. Beyond this, the figure shows how the *Müller et al.* [2016] grid's 0.1° resolution causes closely spaced fracture zones in the equatorial and SE South Atlantic to merge with the result that large areas assume apparent, but artificial, ultraslow seafloor spreading rates. Long-distance interpolations in the Georgia and innermost Argentine basins lead to similar artifacts. Resolution artifacts are much less evident in the grid of spreading rates determined by *Müller* et al. [2008]. One reason for this is that grid's finer (2 arc min) resolution. More importantly however their approach to calculating spreading rates, using stage rotations calculated from the finite rotations on which the age grid is based, is not affected by the rotation of the age gradient that gridding algorithms can cause near age discontinuities. The computation of stage rotations from finite reconstruction parameters tends to be unstable in the face of small finite rotation errors, however, and this instability can

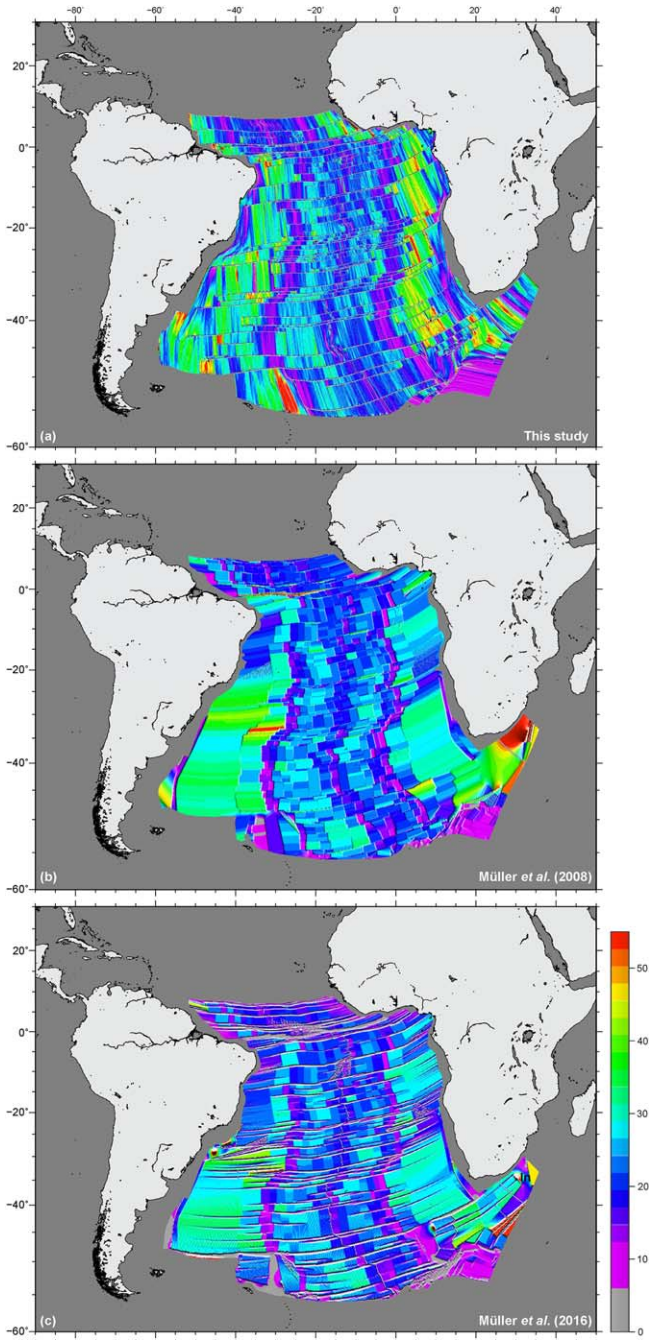

Figure 9. (a) Spreading rates derived from gradients in the age-grid of this study, (b) spreading rates calculated from the age grid of *Müller et al.* [2008], and (c) Spreading rates calculated from the age grid of *Müller et al.* [2016]. Gray scale areas depict ultraslow seafloor spreading rates.

produce artifactual contrasts in conjugate age vectors. That such contrasts may be exposed in Figure 9 can be implied from the visually more marked asymmetries in spreading rates determined by *Müller et al.* [2008, 2016] than from the gradient of our new age grid, which is ultimately based on a set of finite rotations whose calculation is strongly influenced by the addition of stage rotations computed on the basis of the continuity of fracture zone shapes, a constraint that the visual-fit modeling approach of *Nürnberg and Müller* [1991] could not make as full use of.

Another example of the uses for seafloor age grids is in paleobathymetric modeling, as discussed by Pérez Díaz and Eagles (submitted manuscript) whose first step towards modeling South Atlantic paleobathymetry is to produce thermally subsiding surfaces by applying plate-cooling theory [*Stein and Stein*, 1992] using the high-resolution age grid presented here as input. In order to produce meaningful and reliable models, (paleobathymetric or otherwise) it is indispensable to understand the uncertainties in the different data sets used as inputs. By examining and quantifying the factors affecting age grid accuracy, we are able to produce maps of grid uncertainty that highlight areas susceptible to large seafloor age error. These are limited to areas where points of constrained age (magnetic anomaly or kinematic model isochrons) are scarce and/or regions in the vicinity of age discontinuities (such as fracture zone traces and fossil ridge segments). For the remaining 94% of the South Atlantic, uncertainty in the ages depicted by the new grid is $<$10 My (Figure 7). Figure 10 shows what the full range of uncertainties in Figure 7 implies in terms of possible errors in the thermal subsidence contribution to paleobathymetry [*Stein and Stein*, 1992]. Large possible model depth errors are to be expected associated with large age grid uncertainties. As well as this, because thermal subsidence occurs most rapidly where the seafloor is youngest, large areas of large possible errors occur near paleo-spreading ridges, especially those that accommodated fast plate divergence. Combining these conditions, Figure 10 illustrates how the largest (up to 600 m) areas of large errors in paleobathymetry are to be expected in reconstructions of the areas close to the ridge crest during CNS times (e.g., 100 Ma).

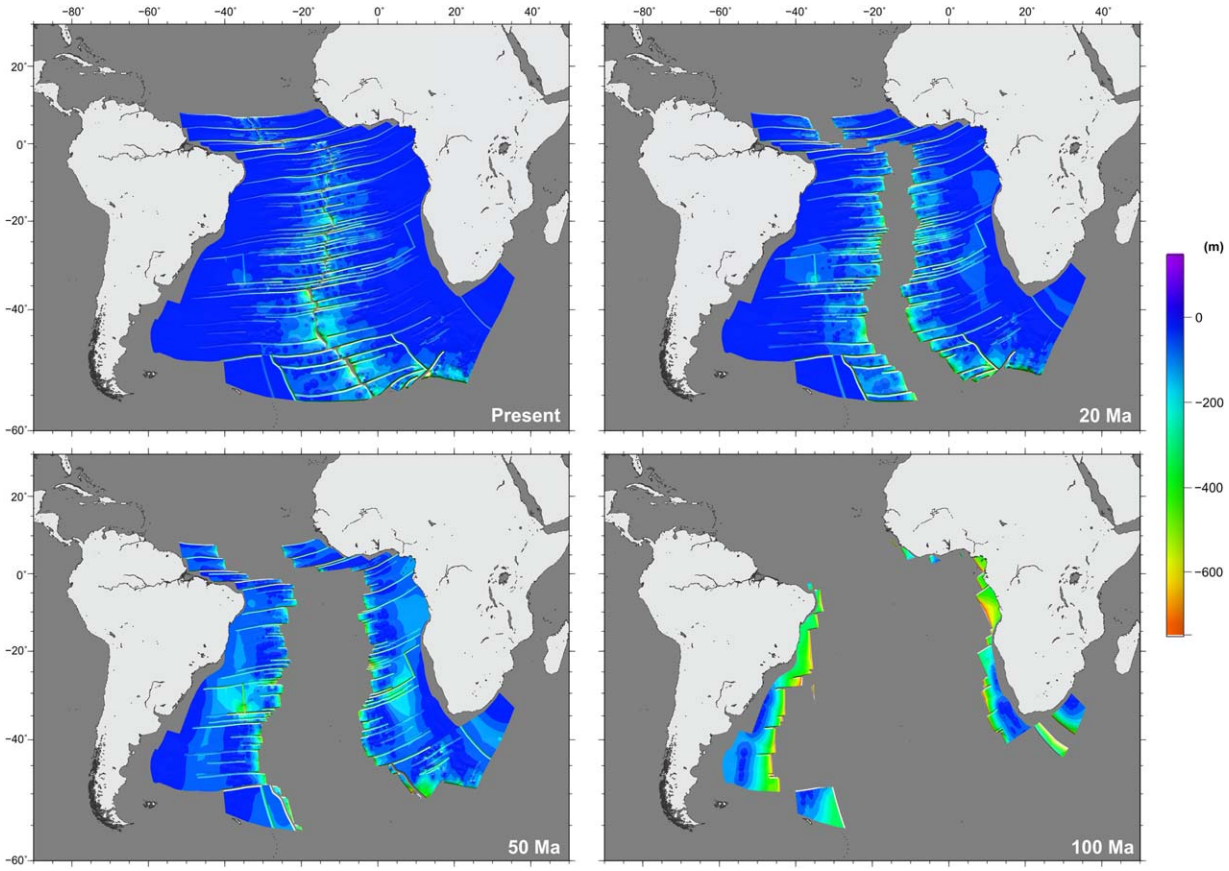

Figure 10. Four determinations of the effect of uncertainty in the age grid in terms of erroneous seafloor depth by thermal subsidence for various paleo-ages (0, 20, 50, and 100 Ma).

Acknowledgments
Data for this paper were obtained from NOAA's Marine Geophysical Trackline Database (magnetic anomaly profiles) and the Global Seafloor Fabric and Magnetic Lineation Data Base Project (magnetic anomaly picks). The 130 new magnetic isochron picks made in helicopter and shipborne data will be added to the GSFML archive after publication. The age, uncertainty, and gradient grids produced will be made available as part of the supporting information for this Technical Report. We are grateful to Royal Holloway University of London and the Alfred Wegener Institute, Helmholtz Centre for Polar and Marine Research for funding. Both authors would like to thank the COMPASS Consortium for further funding support.

References

Baatsen, M., D. J. J. van Hinsbergen, A. S. von der Heydt, H. A. Dijkstra, A. Sluijs, H. A. Abels, and P. K. Bijl (2015), A generalized approach for reconstructing geographical boundary conditions for palaeoclimate modeling, *Clim. Past Discuss.*, *11*(5), 4917–4942.

Brune, S., S. E. Williams, N. P. Butterworth, and R. D. Müller (2016), Abrupt plate accelerations shape rifted continental margins, *Nature*, *536*(7615), 201–204.

Cande, S. C., and D. V. Kent (1995), Revised calibration of the geomagnetic polarity timescale for the Late Cretaceous and Cenozoic, *J. Geophys. Res.*, *100*, 6093–6095.

Cande, S. C., and D. R. Stegman (2011), Indian and African plate motions driven by the push force of the Reunion plume head, *Nature*, *475*(7354), 47–52.

Cande, S. C., J. L. LaBrecque, and W. F. Haxby (1988), Plate kinematics of the South Atlantic: Chron C34 to present, *J. Geophys. Res.*, *93*, 13,479–13,492.

Crough, S. T., W. J. Morgan, and R. B. Hargraves (1980), Kimberlites: Their relation to mantle hotspots, *Earth Planet. Sci. Lett.*, *50*(1), 260–274. doi:10.1016/0012-821X(80)90137-5.

Eagles, G. (2007), New angles on South Atlantic opening, *Geophys. J. Int.*, *168*(1), 353–361, doi:10.1111/j.1365-246X.2006.03206.x.

Eagles, G., L. Pérez-Díaz, and N. Scarselli (2015), Getting over continent ocean boundaries, *Earth Sci. Rev.*, *151*, 244–265.

Gee, J. S., and D. V. Kent (2007), Source of oceanic magnetic anomalies and the geomagnetic polarity time scale, *Treat. Geophys.*, *5*, 455–507.

Gradstein, F., J. Ogg, and A. Smith (2004), A new geologic time scale, with special reference to Precambrian and Neogene, *Episodes*, *27*(2), 83–100.

Gradstein, F. M., et al. (1994), A Mesozoic time scale, *J. Geophys. Res.*, *99*, 24,051–24,074.

Hartnady, C. J., and A. P. le Roex (1985), Southern Ocean hotspot tracks and the Cenozoic absolute motion of the African, Antarctic, and South American plates, *Earth Planet. Sci. Lett.*, *75*(2–3), 245–257, doi:10.1016/0012-821X(85)90106-2.

Heine, C., J. Zoethout, and R. D. Müller (2013), Kinematics of the South Atlantic rift, *Solid Earth Discuss.*, *5*(1), 41–116, doi:10.5194/sed-5-41-2013.

Jokat, W. (2009), The Expedition ARK-XXIII/3 of RV Polarstern in 2008, *Rep. Pol. Mar. Res.*, *597*, 1–221.

Jokat, W. (2013), The Expedition of the Research Vessel *Polarstern* to the Antarctic in 2013 (ANT-XXIX/5), *Rep. Pol. Mar. Res.*, *666*, 1–86.

Kirkwood, B. H., et al. (1999), Statistical tools for estimating and combining finite rotations and their uncertainties, *Geophys. J. Int.*, *137*(2), 408–428, doi:10.1046/j.1365-246X.1999.00787.x.

König, M., and W. Jokat (2006), The Mesozoic breakup of the Weddell Sea, *J. Geophys. Res.*, *111*, B12102, doi:10.1029/2005JB004035.

Larson, R. L., et al. (1985), *Bedrock Geology of the World*, W. Freeman, New York.

Le Roex, A., et al. (2010), Shona and Discovery aseismic ridge systems, South Atlantic: Trace element evidence for enriched mantle sources, *J. Petrol.*, *51*(10), 2089–2120, doi:10.1093/petrology/egq050.

Marks, K. M., and J. M. Stock (2001), Evolution of the Malvinas Plate South of Africa, *Mar. Geophys. Res.*, *22*, 289–302.

Moulin, M., D. Aslanian, and P. Unternehr (2010), A new starting point for the South and Equatorial Atlantic Ocean, *Earth Sci. Rev.*, *98*(1–2), 1–37, doi:10.1016/j.earscirev.2009.08.001.

Müller, R. D., et al. (1991), Depth to basement and geoid expression of the Kane Fracture Zone: A comparison, *Mar. Geophys. Res.*, *13*(2), 105–129, doi:10.1007/BF00286284.

Müller, R. D., W. R. Roest, J. Y. Royer, L. M. Gahagan, and J. G. Sclater (1997), Digital isochrons of the world's ocean floor, *J. Geophys. Res.*, *102*, 3211–3214, doi:10.1029/96jb01781.

Müller, R. D., et al. (2008), Age, spreading rates, and spreading asymmetry of the world's ocean crust, *Geochem. Geophys. Geosyst.*, *9*, Q04006, doi:10.1029/2007GC001743.

Müller, R. D., et al. (2016), Ocean basin evolution and global-scale reorganization events since Pangea breakup, *Annu. Rev. Earth Planet. Sci. Lett.*, *44*, 107–138, doi:10.1146/annurev-earth-060115-012211.

Nankivell, A. (1997), Tectonic evolution of the Southern Ocean between Antarctica, South America and Africa over the past 84 Ma, PhD thesis, Worcester Coll., Univ. of Oxford, Oxford, U. K.

Nürnberg, D., and R. Müller (1991), The tectonic evolution of the South Atlantic from Late Jurassic to present, *Tectonophysics*, *191*, 27–53, doi:10.1016/0040-1951(91)90231-G.

Parmentier, E., and D. Forsyth (1985), Three dimensional flow beneath a slow spreading ridge axis: A dynamic origin of the deepening of the median valley toward fracture zones, *J. Geophys. Res.*, *90*, 678–684.

Pérez-Díaz, L., and G. Eagles (2014), Constraining South Atlantic growth with seafloor spreading data, *Tectonics*, *33*, 1848–1873, doi:10.1002/2014TC003644.

Sandwell, D.T., R. D. Müller, W. H. Smith, E. Garcia, and R. Francis (2014), New global marine gravity model from CryoSat-2 and Jason-1 reveals buried tectonic structure, *Science*, *346*(6205), 65–67.

Schettino, A., and C. R. Scotese (2005), Apparent polar wander paths for the major continents (200 Ma to the present day): A palaeomagnetic reference frame for global plate tectonic reconstructions, *Geophys. J. Int.*, *163*, 727–759, doi:10.1111/j.1365-246X.2005.02638.x.

Sclater, J. G., B. Parsons, and C. Jaupart (1981), Oceans and continents: Similarities and differences in the mechanisms of heat loss, *J. Geophys. Res.*, *86*, 11,535–11,552, doi:10.1029/JB086iB12p11535

Shaw, P., and S. Cande (1990), High-resolution inversion for South Atlantic plate kinematics using joint altimeter and magnetic anomaly data, *J. Geophys. Res.*, *95*, 2625–2644.

Small, C. (1995), Observations of ridge-hotspot interactions in the Southern Ocean, *J. Geophys. Res.*, *100*, 17,931–17,946. doi:10.1029/95JB01377.

Smith, D. K., et al. (1999), Locating the spreading axis along 80 km of the Mid-Atlantic Ridge south of the Atlantis Transform, *J. Geophys. Res.*, *104*, 7599–7612, doi:10.1029/1998JB900064.

Stein, C. A., and S. Stein (1992), A model for the global variation in oceanic depth and heat flow with lithospheric age, *Nature*, *359*(6391), 123–129.

Torsvik, T. H., S. Rousse, C. Labails, and M. A. Smethurst (2009), A new scheme for the opening of the South Atlantic Ocean and the dissection of an Aptian salt basin, *Geophys. J. Int.*, *177*(3), 1315–1333, doi:10.1111/j.1365-246X.2009.04137.x.

Wessel, P., K. J. Matthews, R. D. Müller, A. Mazzoni, J. M. Whittaker, R. Myhill, and M. T. Chandler (2015), Semiautomatic fracture zone tracking, *Geochem. Geophys. Geosyst.*, *16*, 2462–2472, doi:10.1002/2015GC005853.